Supplementary Information

Supplementary Figure 1 Linearity of gap gene antibody stainings.

Supplementary Figure 2 Reduction of gene expression profile variance due to time correction and residual variance due to measurement error in δ_{FC}.

Supplementary Figure 3 Systematic error contributions due to noise in the imaging process, and due to non-specificities of primary and secondary antibodies

Supplementary Figure 4 Contribution of azimuthal embryo orientation uncertainty to Gt gene expression profile reproducibility (alternative method).

Supplementary Figure 5 Contribution of azimuthal embryo orientation uncertainty to gap gene expression profile reproducibility.

Supplementary Figure 6 Influence of the age and orientation window on the reproducibility of the markers.

Supplementary Figure 7 Positional error for two genes.

Supplementary Figure 1: Linearity of gap gene antibody stainings. An embryo containing a Gt-YFP fusion protein was formaldehyde fixed at approximately 40 min into n.c. 14, stained with a guinea pig anti-Gt primary antibody and an Alexa-647 conjugated secondary antibody, and imaged via confocal microscopy. **A)** Image of Gt antibody immunofluorescence; scale bar is $100\,\mu m$. **B)** Image of YFP autofluorescence of same embryo as in A. Yellow square in A and B corresponds to a 50×50 pixel window used to determine background intensity. **C)** Scatter plot of raw nuclear intensities, in gray, and their binned average (black) computed over 15 equally populated bins (see Supplementary Materials). Red dot shows mean intensity measured in yellow square in A and B. Standard deviations for each bin are smaller than the width of the black and red dots.

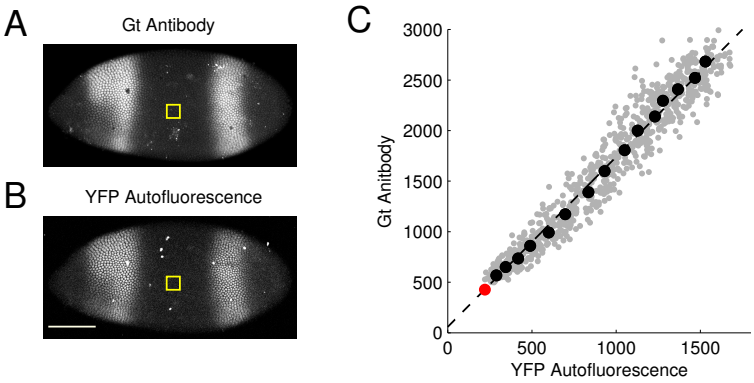

Supplementary Figure 2: Reduction of gene expression profile variance due to time correction and residual variance due to measurement error in δ_{FC}. **A)** Comparison of the time-corrected (dark colors) and non-time-corrected (light colors) variances in gene expression for each gap gene computed over 23 embryos (DV orientation only, $\delta_{\mathrm{FC}} = 10 - 20$ μm). Error bars have been obtained by exhaustively bootstrapping over all subsets of $n-1$ embryos. **B)** For each gap gene, the estimate of the residual time variance $\sigma_{g_{\mathrm{age}}}$ due to the uncertainty (± 1 μm) on the measure of δ_{FC} is shown in gray (see also Materials and methods). For reference, the variances of the time-corrected normalized profiles is shown in dark colors.

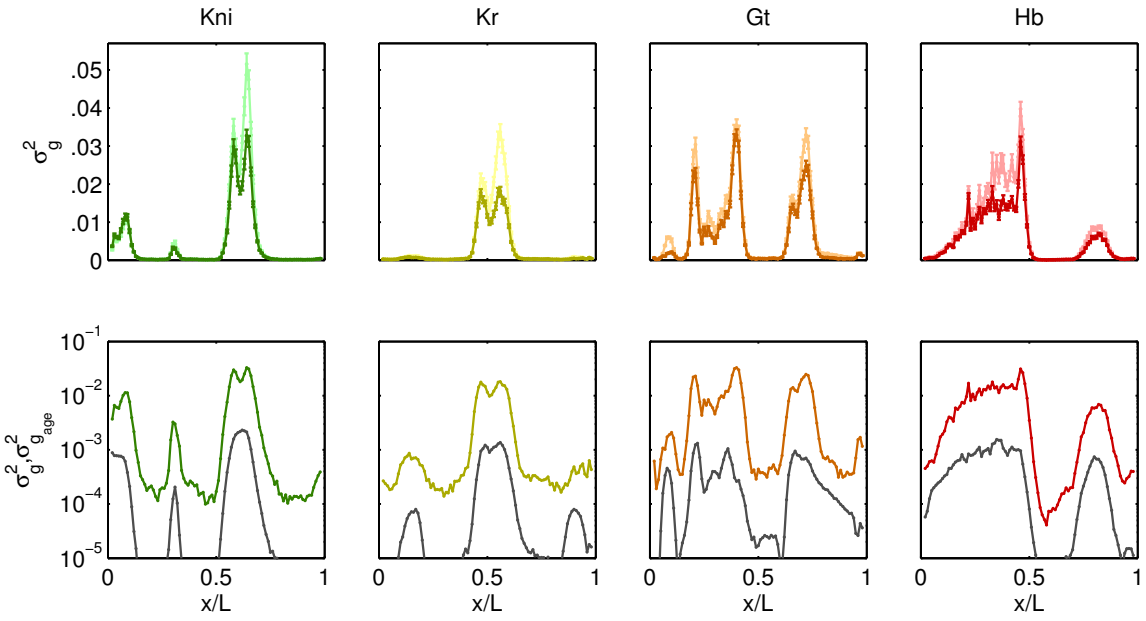

Supplementary Figure 3: Systematic error contributions due to noise in the imaging process, and due to non-specificities of primary and secondary antibodies. An embryo, heat fixed approximately 40 min into n.c. 14, was stained with two different primary antibodies (rat and guinea pig anti-Hb) and three different secondary antibodies (Alexa conjugated 488 anti-rat, 546 anti-guinea pig, 647 anti-guinea pig). Embryo imaged in three different channels via confocal microscopy can be seen at top (green-488, yellow-546, red-647). **A-C)** Scatter plots of the raw nuclear intensities (712 nuclei) from two independent successive imaging sequences, taken in the same channel (light colored dots, repeat sequence on the y-axis). Blue dots represent the measurement of the background, performed by averaging the intensity over 10 nuclear size masks randomly selected in the 60-70%EL region of the embryo. The dark color lines are linear fits to the raw nuclear intensities, and the black dashed line corresponds to equal intensities on the x- and y-axis (slope=1). Insets show intensity measurement noise σ_I as a function of mean intensity computed across 40 equally spaced bins along the full intensity spectrum. For consistency only bins with 10 or more points are shown. **D)** Scatter plot of the nuclear intensities from channels with different primary and secondary antibodies (anti-rat(488) and anti-guinea pig(546)). Two dashed lines show were the zero and one levels of gene expression are determined. Inset shows the measurement noise of the intensity as a function of the mean intensity. **E)** Scatter plot of the nuclear intensities from channels with different secondary antibodies (anti-guinea pig(546) and anti-guinea pig(647)). Inset as in D.

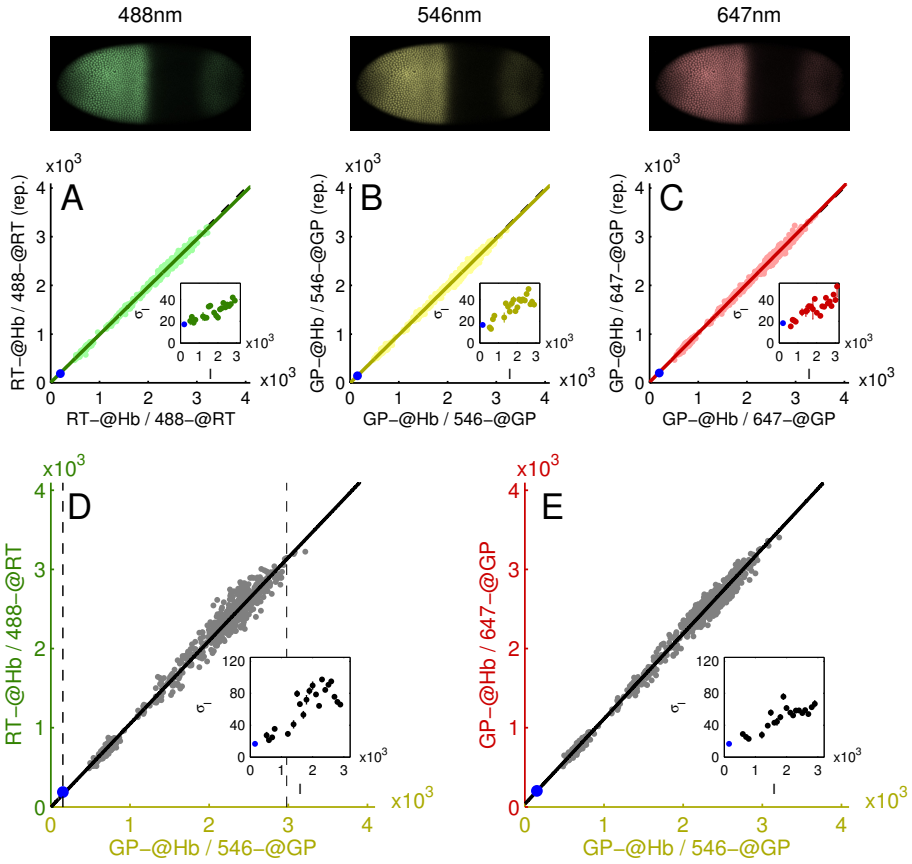

Supplementary Figure 4: Contribution of azimuthal embryo orientation uncertainty to Gt gene expression profile reproducibility (alternative method). The dorsal side of a flattened embryo (fixed 40 min after the onset of n.c. 14 (FC depth = 12μm) and immunostained against *kni*, *kr*, *gt* and *hb*) was imaged. **A)** Nuclear mask of the embryo. Each nucleus was assigned an 'angle' ϕ defined as $y/y_{\max}$, where y is the y-coordinate of the nucleus and $y_{\max}$ the y-coordinate of the outline (in black) at the same AP position (x-coordinate). The nuclei were then sorted according to 10° bins and color coded according to their bin (from red to blue). **B)** Gt profiles for each bin. **C)** Dependence of intensity on angle. Intensity measured in each bin is plotted for $x/L = 0.38$ (□) and $x/L = 0.55$ (○). Typical eye-selection allows for discrimination of embryos for which the midsagittal plane lies within $-40° < \phi < 40°$ (black lines). **D)** Mean and standard deviation of Gt intensity profiles computed across the the 7 profiles in the $-40° < \phi < 40°$ bin. The minimum and maximum mean intensities in the 20-80%EL region are shown as dashed lines (defining the minimum (0) and maximum (1) gene expression levels, respectively). Inset shows the standard deviation as a function of the mean for 100 equally spaced points along the AP-axis, with the blue dot representing the standard deviation of the background intensity. **E)** Variance of the 7 previous profiles plotted as a function of the fractional length (dashed gray line); total variance of gene expression profiles of the time corrected dorsal profiles is shown in dark orange for comparison

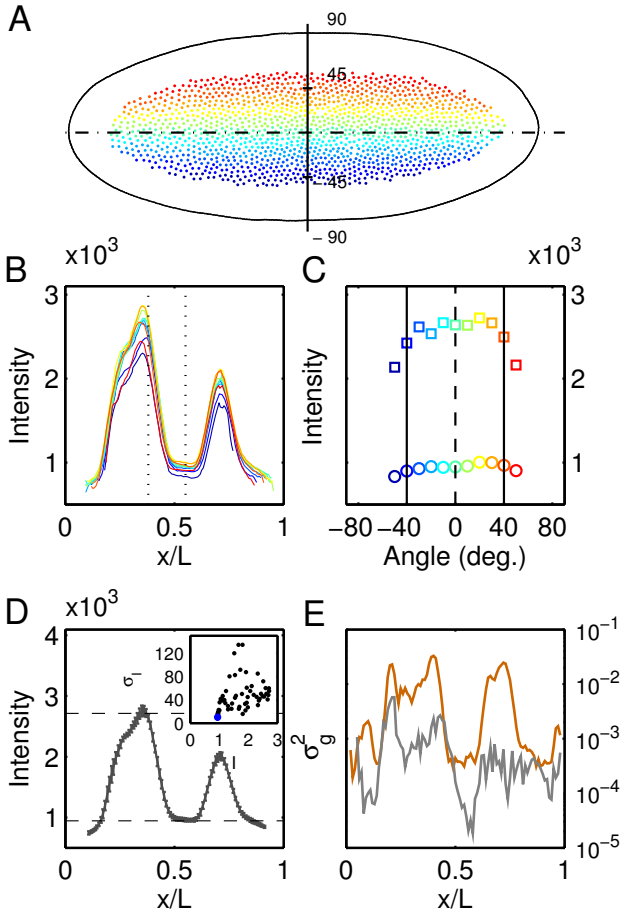

Supplementary Figure 5: Contribution of azimuthal embryo orientation uncertainty $\sigma^2_{g_\phi}$ to gap gene expression profile reproducibility σ^2_g. For each gap gene, the estimate of the variance due to the uncertainty on the measure of the orientation of the embryo (logarithmic scale) is shown as a function of x/L; estimated as in **Figure 4** (black plain line) and as in **Supplementary Figure S4** (gray line). The variances of the time-corrected normalized profiles are shown as a reference in dark colors.

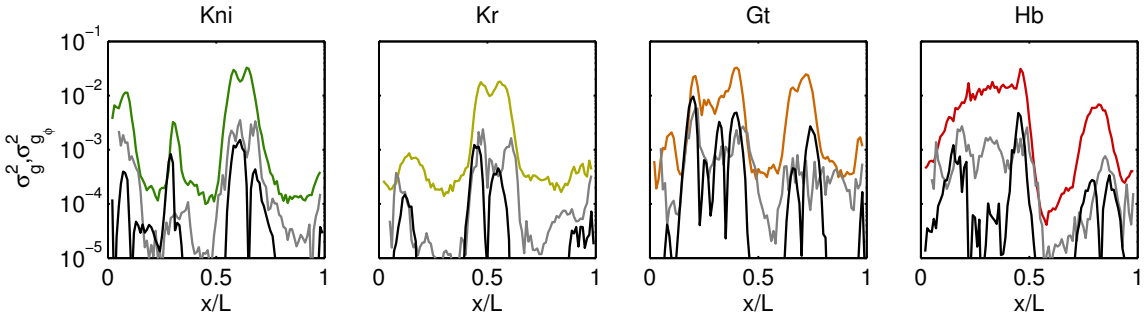

Supplementary Figure 6: Influence of the age and orientation window on the reproducibility of the markers. **A)** Reproducibility of various dorsal markers depending on their position along the anteroposterior axis for 163 embryos without prior selection for age and orientation (grey) and 10 embryos selected to be 41 to 45 min into n.c. 14 (time class T6), and oriented in the midsagittal plane (blue). The average standard deviation of the positions across markers corresponds to half the internuclear distance (1.6 μm), shown as a dashed line as depicted on panel A. **B)** Schematic representation of the reproducibility of a border across profiles and how it relates to the internuclear distance.

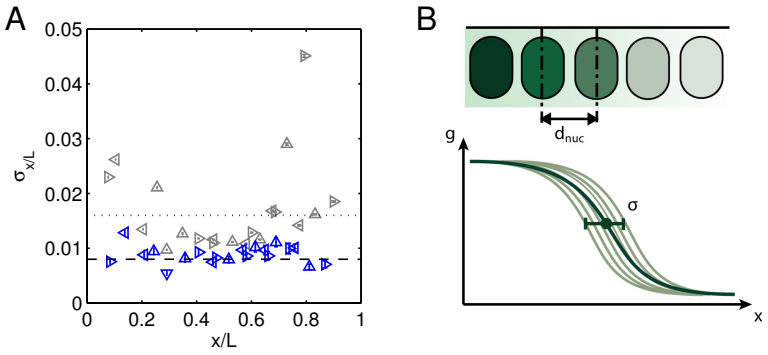

Supplementary Figure 7: Positional error for two genes. **A)** Mean dorsal Hb profile and standard deviation ($10 < \delta_{\mathrm{FC}} < 20\,\mu$m, 23 embryos) as a function of fractional egg length x/L. The inset shows a close-up of the transition region with the positional error $\hat{\sigma}_x$ geometrically determined by reading out the mean $\bar{g}(x)$ and the standard deviation σ_g of the profiles. **B)** Positional error in reading out Hb as a function of x/L, computed using $\hat{\sigma}_x(x) = \sigma_g \cdot |dg/dx|^{-1}$, for 100 bins along the AP axis. For reference, the internuclear distance and half-internuclear distance are shown in dotted and dashed lines, respectively. Error bars are obtained by bootstrapping 10 times over $\mathcal{N}/2$ embryo subsets. **C)** Mean profile and standard deviation for Kr from the same data set as in A. **D)** Positional error in reading out Kr as a function of x/L (equivalent to B). **E)** Three-dimensional representation of Hb and Kr profiles from A and C as a function of relative position. Gray curve shows the mean and standard deviations in the Hb − Kr plane, i.e. their joint distribution. Black curve shows the joint Hb − Kr mean expression as a function of x/L. **F)** Positional error $\hat{\sigma}_x$ for the Hb − Kr pair using their mean expression and covariance shown in E (see Supplementary Materials).